The Astrophysical Journal Letters, 781:L7 (5pp), 2014 January 20 doi:10.1088/2041-8205/781/1/L7

IMPLICATIONS OF THE RECENT LOW SOLAR MINIMUM FOR THE SOLAR WIND DURING THE MAUNDER MINIMUM

M. Lockwood and M. J. Owens
Department of Meteorology, University of Reading, Earley Gate, RG6 6BB, UK; m.lockwood@reading.ac.uk
Received 2013 November 18; accepted 2013 December 5; published 2013 December 23

ABSTRACT

The behavior of the Sun and near-Earth space during grand solar minima is not understood; however, the recent long and low minimum of the decadal-scale solar cycle gives some important clues, with implications for understanding the solar dynamo and predicting space weather conditions. The speed of the near-Earth solar wind and the strength of the interplanetary magnetic field (IMF) embedded within it can be reliably reconstructed for before the advent of spacecraft monitoring using observations of geomagnetic activity that extend back to the mid-19th century. We show that during the solar cycle minima around 1879 and 1901 the average solar wind speed was exceptionally low, implying the Earth remained within the streamer belt of slow solar wind flow for extended periods. This is consistent with a broader streamer belt, which was also a feature of the recent low minimum (2009), and yields a prediction that the low near-Earth IMF during the Maunder minimum (1640–1700), as derived from models and deduced from cosmogenic isotopes, was accompanied by a persistent and relatively constant solar wind of speed roughly half the average for the modern era.

Key words: solar–terrestrial relations – solar wind – Sun: activity – Sun: corona – Sun: magnetic fields

Online-only material: color figures

1. INTRODUCTION

During the Maunder minimum (MM), almost no sunspots were detected, as shown by Figure 1. In recent years we have started to gain some insight into the space weather conditions during this interval and that is helping to inform predictions for the future (Barnard et al. 2011). That solar activity was very low in the MM has been confirmed by observations of high abundances of cosmogenic isotopes, namely ^{14}C and ^{10}Be stored in terrestrial reservoirs (Usoskin 2013). These isotopes also show that this was the most recent of a series of "grand solar minima" (Steinhilber et al. 2010) and our understanding of the solar dynamo will be inadequate until we understand how these grand minima arise. The cosmic ray flux that generates cosmogenic isotopes is higher when the open solar magnetic flux (OSF, the magnetic flux leaving the top of the solar corona and filling the heliosphere) is lower and so also varies inversely with the heliospheric magnetic field. From the theory of this relationship, the average near-Earth interplanetary magnetic field (IMF) in the MM has been estimated to have been $B = 1.80 \pm 0.59$ nT (Steinhilber et al. 2010), considerably smaller than the average observed by spacecraft over the last four solar cycles ($\approx$6 nT). Models using the sunspot number to quantify the emergence rate of open magnetic flux from the Sun (Solanki et al. 2000) reproduce the variation deduced from geomagnetic observations (Lockwood et al. 1999; Lockwood et al. 2009), and Figure 1 shows a modeled variation, $B_{\rm m}$, that averages about 2 nT in the MM (Owens & Lockwood 2012). This model allows for a base-level emergence of OSF in continued coronal mass ejection (CME) release during the MM at the rate that was observed during the recent long and low minimum to the decadal-scale solar cycle. In addition, a cycle-dependent loss rate of open flux, set by the degree of warping of the heliospheric current sheet (Owens et al. 2011), explains an otherwise anomalous phase relation between the isotopes and sunspot numbers at the start and end of the MM (Owens et al. 2012). However, none of these studies tell us about the speed of the solar wind, $V_{\rm SW}$, which was incident on the Earth during the MM.

2. RECONSTRUCTION OF THE IMF AND SOLAR WIND SPEED SINCE 1868

A variety of geomagnetic indices have been derived which monitor different parts of the magnetosphere–ionosphere current system induced by the flow of magnetized solar wind plasma past the Earth (see recent review by Lockwood 2013). An important insight is that a dependence of geomagnetic activity on the solar wind speed $V_{\rm SW}$ is introduced by the substorm current wedge (Finch et al. 2008), a fact well explained by the effect of solar wind dynamic pressure on the near-Earth tail of the magnetosphere (Lockwood 2013). Consequently, geomagnetic indices such as *aa* and *IHV* that are strongly influenced by substorms, vary as $BV_{\rm SW}^n$ with n close to 2. On the other hand, interdiurnal variation indices such as *IDV* and *IDV(1d)* (recently introduced by Lockwood et al. 2013a) are dominated by the ring current and give $n \approx 0$. These differences in n are statistically significant (Lockwood et al. 2009) and hence combinations of indices can be used to infer both B and $V_{\rm SW}$ (Svalgaard et al. 2003; Rouillard et al. 2007; Lockwood et al. 2009). The interplanetary data used here are for 1966–2012, inclusive, and correlations are carried out on annual means. The geomagnetic indices used are $aa_{\rm C}$, *IDV*, *IDV(1d)*, and *IHV* (see descriptions by Lockwood 2013). Svalgaard (2013) has pointed out that the *IDV(1d)* index for much of solar cycle 11 is too small and we here use the *IDV(1d)* series presented by Lockwood et al. (2014) that uses St Petersburg data and a comparison of *k* indices with the *aa* index to make the required correction.

The peak linear correlations of each index with $BV_{\rm SW}^n$, r, and the optimum n values, are given in Table 1. The largest correlation possible for annual means and $n = 0$ is 0.95 (and for $n = 2$ is 0.97) because geomagnetic activity is driven by the

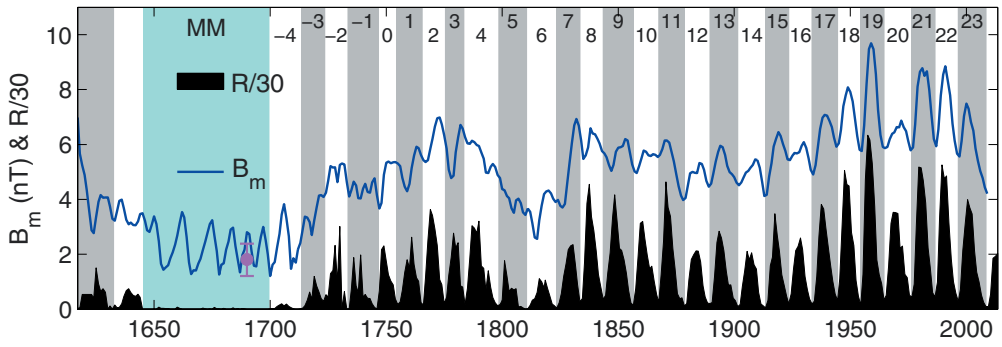

Figure 1. Variation of sunspot numbers, R (black shaded area), and modeled near-Earth IMF, B_m (blue line). Even- and odd-numbered solar cycles are shaded white and gray and the Maunder minimum (MM) is in cyan. R is the international sunspot number extended back to before the MM using a linear regression of the group sunspot number ($R/30$ is shown to allow use of a common vertical scale). B_m is derived from the OSF modeled from R using the continuity equation (Owens & Lockwood 2012), which is subsequently converted into near-Earth IMF using an empirical relationship (Lockwood et al. 2009; Lockwood 2013). The mauve point and error bar is the estimate of IMF for the end of the MM from cosmogenic isotopes (Steinhilber et al. 2010).

(A color version of this figure is available in the online journal.)

Table 1
The Peak Linear Correlation Coefficients, r, and the Optimum n Values for the Geomagnetic Indices with BV_{SW}^n

Index	r	n
aa_C	0.961	1.7
IDV(1d)	0.919	−0.1
IDV	0.908	−0.1
IHV	0.944	1.9

southward component of the IMF in the Earth's magnetic frame and the orientation factor does not quite average to a constant on annual timescales (Lockwood 2013). The correlations in Table 1 are not far short of these maximum possible values.

Figure 2(a) shows the variation of international sunspot number R over the interval studied in the present Letter. For this interval, both V_{SW} and B can be reconstructed using pairs of indices giving different n. The results are shown in Figures 2(c) and (e). The agreement in Figure 2(c) between all four reconstructions for V_{SW} is very high: note that V_{SW} falls below 300 km s^{-1} in 1902 (solar minimum 13/14) for all four reconstructions. The aa_C-*IDV* and aa_C-*IDV(1d)* reconstructions extend back to 1868 and show similarly low V_{SW} in the minimum 11/12 (around 1879). Comparison with the distributions shown in Figure 2(d) reveals that V_{SW} was lower in these minima than any annual means seen during the space age and very similar to the lowest values seen in hourly means. Figure 2(e) shows excellent agreement between B from the various combinations of indices and good general agreement with the modeled variation B_m shown in Figure 1. All reconstructed and modeled IMF variations are always within the uncertainty band computed by Lockwood et al. (2013b) from a Monte Carlo error analysis of the reconstructions, once the correction to *IDV(1d)* for cycle 11 is made (Lockwood et al. 2014). In Figures 2(c) and (e) both the annual median and mean values of the in situ observations are given: in general, the almost constant offset between the two shows that the annual distributions of B and V_{SW} maintain a relatively constant shape. The biggest exception to this are the large peaks in V_{SW} when medians and means become similar, revealing a more symmetric distribution. Figure 2(b) is a scatter plot of the reconstructed V_{SW} against reconstructed B (points color-coded as in Figures 2(c) and (e)) and shows that annual means of V_{SW} decrease rapidly at the lowest B (below about 5 nT). This offers two possibilities: (1) either the minimum (hourly mean) V_{SW} was lower than it has been at any time during the space age or (2) the slow solar wind has not changed but Earth spent more extended intervals within it. In this Letter we concentrate on effect (2) but here first briefly consider effect (1). Schwadron & McComas (2003) explain the observed anticorrelation between solar wind speed and source coronal temperature and deduce a minimum solar wind speed of about 200 km s^{-1}, below which the source wind becomes subsonic and hence bound. Average coronal temperatures, mean (Sun-as-star) photospheric field magnitude, B_P, and associated integral soft X ray emission are all expected to be smaller at lower solar activity (Pevtsov et al. 2003; Schwadron et al. 2006; Riley et al. 2010) which would give faster average solar wind under this scaling relation, although we note that from soft X-ray emissions from two putative stellar analogues of the MM Sun, Judge & Saar (2007) find no evidence for this. From all of the above we conclude that effect (1) is unlikely as a cause of the low V_{SW} deduced for solar minima 11/12 and 13/14.

3. RECENT SOLAR MINIMA

An important clue is provided by recent solar cycle minima, when Earth has tended to spend intervals in the fast solar wind (as illustrated schematically in Figure 3(a)) which raises the annual means and also means that some of the near-Earth slow solar wind is accelerated to intermediate speeds by co-rotating interaction regions where fast wind catches up with the slow wind ahead. The similarity of the annual mean V_{SW} in minima 11/12 and 13/14 to the lowest observed hourly means in recent cycles strongly suggests that Earth remained within slow SW for extended intervals during these minima and that the slow solar wind source regions were as hot as in recent solar cycles so that the average speed of the slow solar wind was as low as it has been during the space age.

Supporting evidence for this idea comes from the behavior during solar minimum 23/24, when Earth spent a larger fraction of time in the slow solar wind, and mean V_{SW} values were therefore lower (Cliver & Ling 2011; de Toma 2011). Figure 4(d) shows the streamer belt width, defined as where dipole streamers and pseudostreamers are detected using magnetograph data and the potential field source surface modeling by the method described by Owens et al. (2013, 2014). This belt decreased in latitudinal width over all three declining phases of the observed solar cycles, but did not become as thin during minimum 23/24 as it had at the previous two minima. Both types of streamer

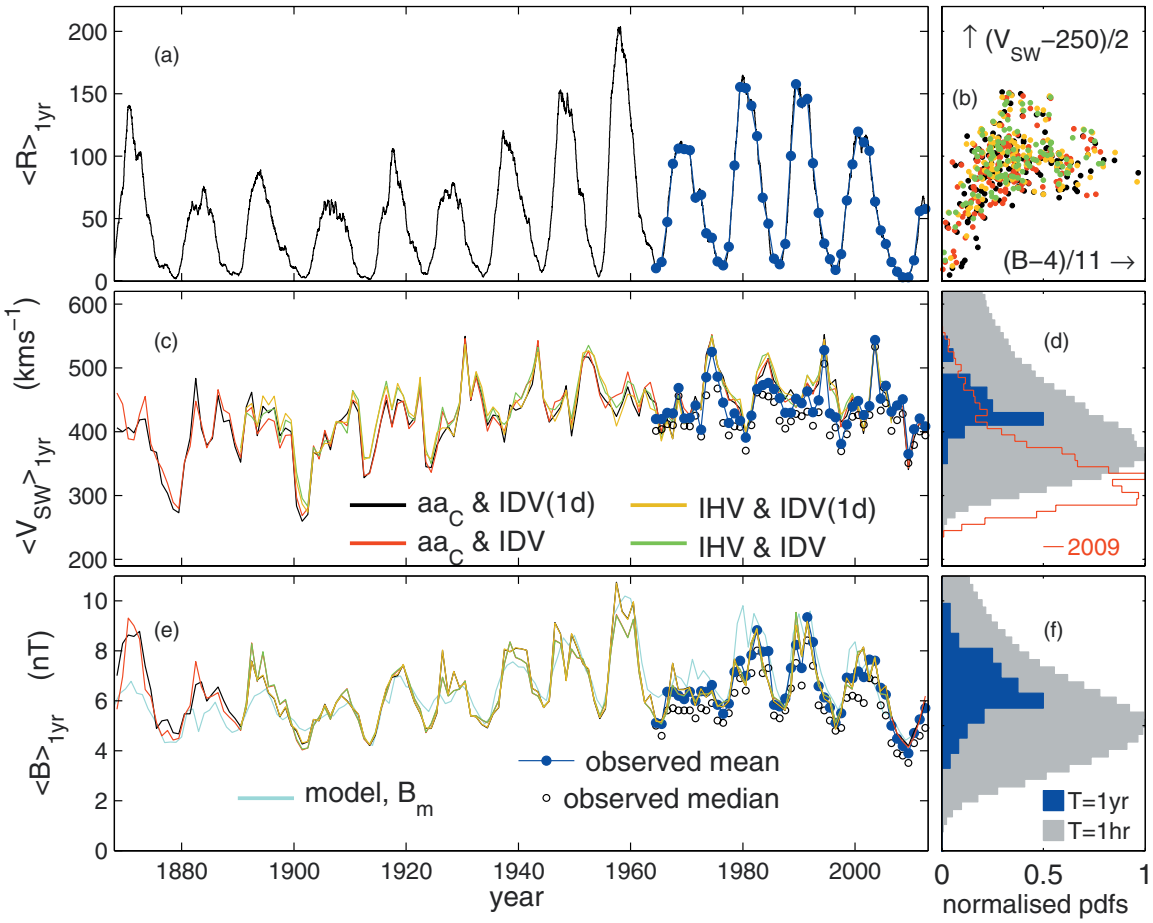

Figure 2. (a): 12-point running means of monthly international sunspot numbers, $\langle R \rangle_{1yr}$. (c) and (e): Reconstructed annual near-Earth SW speed $\langle V_{SW} \rangle_{1yr}$ (panel (c)) and IMF $\langle B \rangle_{1yr}$ (panel (e)) from the various pairings of geomagnetic indices. The blue filled and black open dots give annual mean and median values, respectively, of satellite observations and the cyan line in panel (e) is the modeled field B_m shown in Figure 1. (d) and (f): normalized distributions of hourly (in gray) and annual (in blue) means of V_{SW} (panel (d)) and B (panel (f)), observed during the space age (note that the pdf scale has been halved for annual values for clarity). Panel (d) also shows the distribution of hourly V_{SW} means for the calendar year 2009. (b): $\langle V_{SW} \rangle_{1yr}$ as a function of $\langle B \rangle_{1yr}$. In panels (b), (c), and (e), black, red, orange, and green are for reconstructed values from the pairings of, respectively, *IDV(1d)* − aa_C, *IDV* − aa_C, *IDV(1d)* − *IHV*, and *IDV* − *IHV*.

(A color version of this figure is available in the online journal.)

act as sources of the slow solar wind (Riley & Luhmann 2012; Owens et al. 2013, 2014). The increased width of the streamer belt in the minimum 23/24, compared to minimum 22/23, has also been inferred from the Thompson-scattered light from the solar corona, as detected by coronagraphs, and from interplanetary scintillation observations of the solar wind (Manoharan 2012). The wider the streamer belt, the lower the chance that warps in the current sheet and/or the annual 14 deg variation of the Earth's heliographic latitude can take it out of the streamer belt and into fast or intermediate solar wind. Thus we would expect lower mean speeds and reduced variability in the solar wind at sunspot minimum if the IMF is low. Panels (a)–(c) of Figure 4 show, respectively, the near-Earth IMF B, the mean (Sun-as-a-star) of the magnitude of the photospheric field B_P and V_{SW} in both Carrington rotation means (gray) and annual means (black). Annual means of B for minima 21/22, 22/23, and 23/24 were 5.76 nT, 5.11 nT, and 3.89 nT, respectively. Corresponding values of B_P were 9.31 μT, 9.11 μT, and 3.87 μT and for V_{SW} were 429 km s^{-1}, 381 km s^{-1}, and 336 km s^{-1}. Thus all three have fallen over the last three solar cycle minima with B_P in minimum 23/24 being less than half that in the previous two minima. A continuation of this trend is consistent with the very slow wind speeds deduced here for minima 11/12 and 13/14.

4. SUNSPOT MAXIMUM AND THE IMF AT THE PREVIOUS MINIMUM

Further evidence that minima 11/12 and 13/14 were rather similar to minimum 23/24 comes from comparing the subsequent sunspot maxima (12, 13, and 24). Cycle 24 appears to have recently passed its maximum (Lockwood 2013) giving a peak 1-yr mean sunspot number of $R_{max} = 67.5$, very close to, and at the lower end of the uncertainty band of, the 75 ± 8 predicted from the precursor method using solar polar fields at minimum 23/24 by Svalgaard et al. (2005). Because the polar fields at sunspot minima are closely related to the near-Earth IMF, B, this implies a relationship between R_{max} and the IMF in the preceding solar minimum, B_{min}. A polynomial fit to the data in Figures 2(a) and (e) gives

$$R_{max} = 7.352 B_{min}^2 - 19.523 B_{min} + 8.729, \quad (1)$$

where B_{min} is in nT. Equation (1) gives predictions of R_{max} accurate to within 15% for the whole interval shown in Figure 2 (solar cycles 11–24). To within this error, the R_{max} of cycles 12, 13, and 24 (75.7, 64.7, and 67.5) are approximately the same, implying similar prior B_{min} values. Thus the minimum 23/24 provides a useful analogue of the minima 11/12 and

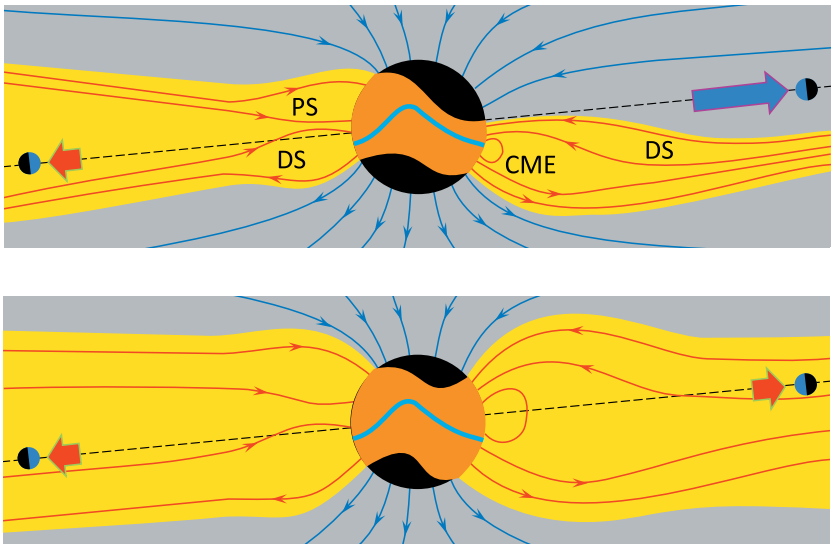

Figure 3. Schematics of the solar atmosphere and interplanetary space at sunspot minimum, viewed in a reference frame co-rotating with the solar corona with two snapshots of the Earth's location, half a solar rotation period apart. The black areas in the solar atmosphere are the unipolar polar coronal holes from which open magnetic flux (blue lines) and the lower-temperature, fast solar wind emerges. The yellow area is the streamer belt where hotter, slow solar wind emerges from both dipolar streamers (DS) or pseudostreamers (PS), in which field lines, shown in red, of opposite and same polarity meet, respectively. The light blue line is the base of the heliospheric current sheet. The dashed line is the ecliptic plane. The top panel is typical of recent solar minima, the left half shows slow solar wind (red arrow) impinging on the Earth and the right shows the situation half a rotation later when Earth is in the fast solar wind (blue arrow). (Also note that a coronal mass ejection (CME) is shown emerging along the streamer belt). The bottom panel shows a grand solar minimum with a lower open solar flux but continued base-level CME emergence giving a broader streamer belt.

(A color version of this figure is available in the online journal.)

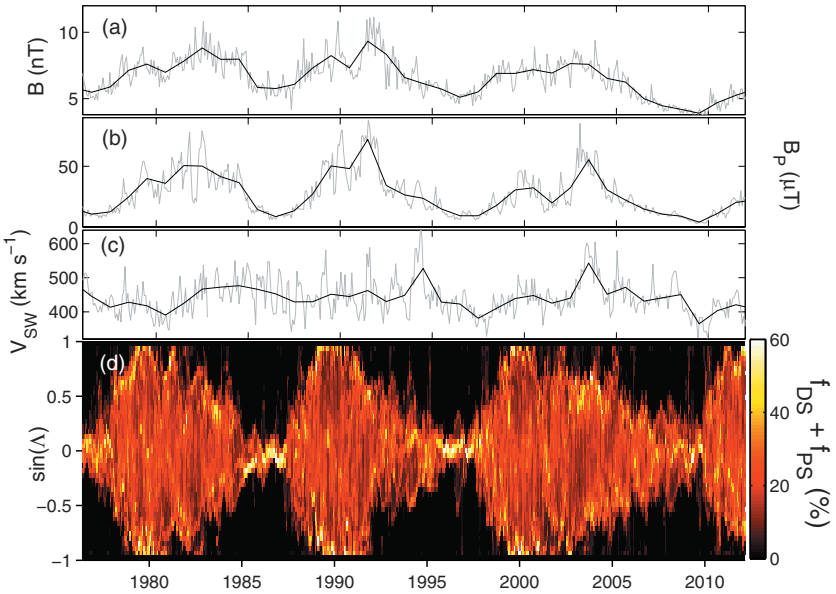

Figure 4. (a)–(c) show, respectively, the near-Earth IMF B, the mean (Sun-as-a-star) photospheric field magnitude B_P and the near-Earth solar wind speed V_{SW} in both Carrington rotation (gray) and annual (black) means. In (d) color contours are shown of Carrington Rotation means of the occurrence frequency (in%) of streamers (both dipolar and pseudostreamers from Potential Field Source Surface modeling of the corona using Wilcox Solar Observatory magnetograms) as a function of heliographic latitude Λ and time. Streamers are defined by $\log_{10}(dS_{PH}/dS_{SS}) > 1$ where dS_{PH} is the separation of a pair of field lines in the photosphere and dS_{SS} their separation at the coronal source surface (Owens et al. 2013, 2014).

(A color version of this figure is available in the online journal.)

13/14. The red line in Figure 2(f) shows the distribution of hourly V_{SW} values for the year 2009 (minimum 23/24): it reveals predominantly slow, some intermediate, but no fast solar wind (de Toma 2011). Thus the low annual mean for 2009 (the lowest since in situ observations began) can be attributed to a absence of fast solar wind, the relative absence of intermediate solar wind and prolonged residence of Earth in the slow solar wind of the streamer belt.

5. STREAMER BELT WIDTH

At sunspot minimum, the width of the streamer belt is set by its open solar flux (OSF) contribution, relative to that of the polar coronal holes. Because of the latitudinal constancy of tangential magnetic pressure in the solar wind as it leaves the corona, the belt will expand or contract in latitude to equalize the magnitude of the radial magnetic field at all latitudes, as found

by the *Ulysses* satellite (see review by Lockwood 2013). This gives Equation (2) for the latitudinal half-width of the streamer belt, Λ_{SB}:

$$\Lambda_{SB} = \sin^{-1}\left\{1 - B_{CH}A_{CH}\Big/\left(4\pi R_1^2\left|B_r\right|_{1day}\right)\right\} \qquad (2)$$

where $|B_r|_{1day}$ is the radial IMF component measured R_1 from the Sun: taking the modulus of 1 day means gives a good total unsigned OSF estimate of $4\pi R_1^2|B_r|_{1day}$ (Lockwood et al. 2009; Lockwood 2013). A_{CH} is the total area of the two polar coronal holes and B_{CH} is the mean field within them. At the last three solar minima, B_{CH} was observed by the Wilcox Solar Observatory to be 126 μT, 92 μT, and 50 μT in annual means (Lockwood et al. 2012), the near-Earth IMF (Figure 4(a)) was 5.55 nT, 5.10 nT, and 3.87 nT while $|B_r|_{1day}$ was 2.28 nT, 1.91 nT, and 1.14 nT (Lockwood 2013). From coronal images, estimates for A_{CH} for the combined polar caps was 10.2% ± 0.5% of the photosphere in 2009 compared to 15.0% ± 0.2% for 1996 (de Toma 2011). Thus for minimum 23/24 B_{CH}, A_{CH}, and $|B_r|_{1day}$ were, respectively, 54%, 68%, and 60% of their values during minimum 22/23. From Equation (2) this means that a value of $\Lambda_{SB} = 5.^\circ7$ ($\sin\Lambda_{SB} = 0.1$) for minimum 22/23 would become $26.^\circ4$ ($\sin\Lambda_{SB} = 0.44$) for minimum 23/24. This is broadly consistent with the change seen in Figure 4(d).

The modeling by Owens & Lockwood (2012) offers an explanation of this broadening. The decreases in B_{CH}, A_{CH}, and $|B_r|_{1day}$ all reflect reduced emergence of open flux (compared to the loss rate) and its transport into the polar coronal holes over cycle 23. On the other hand, at the minima, the observed CME rate was unchanged, suggesting a continued base-level injection of open flux into the streamer belt. In addition, the modeling uses an open flux loss rate that varies with the current sheet tilt and this too reaches a base-level rate at both sunspot minimum. This combination of a base-level emergence and a cycle-dependent loss was invoked to explain the anomalous phase relation between cosmogenic isotopes and sunspot numbers around the MM (Owens et al. 2012). The model predicts that over the last three cycles the open flux in the polar coronal holes at solar minimum has decayed, but the open flux in the streamer belt at those times has remained roughly constant. Therefore the sunspot-minimum streamer belt must have increased in width.

6. THE INFERRED SOLAR WIND DURING THE MAUNDER MINIMA

The minima 11/12, 13/14, and 23/24 are roughly equivalent with B_{min} around 4 nT in each case and the subsequent R_{max} between 65 and 76. This gives a streamer belt just wide enough for the Earth to remain in the slow SW for extended intervals (3 yr in the case of minimum 11/12, 2 yr for 13/14, and 0.5 yr for 23/24). During the MM, B_{min} falls to near 2 nT on average and R_{max} to zero. This would yield an even broader streamer belt from which Earth would not emerge for the full duration of the grand minimum. Hence the Earth would have never intersected fast solar wind. The work of Owens et al. (2012) strongly suggests that the magnetic cycle continued throughout the MM and that, unlike more active cycles, OSF loss rate variations dominated over the production rate cycle, giving peak OSF at the cycle minima during the MM. At the minima of these cycles within the MM we would expect to see persistent slow solar wind as Earth remains within the broad band of slow solar wind and, because of the low values deduced for sunspot minima 11/12 and 13/14, we postulate that solar wind remains slow because it continues to emanate from hot parts of the corona even in the absence of active sunspot regions (from the scaling relation of Schwadron & McComas 2003). At other phases of these cycles in the MM, low latitude coronal holes may form, as in recent cycles, and give fast wind at the latitude of Earth but these would interact with the slow wind ahead of them to give periods of intermediate speed. However, the model predicts that away from the activity minima in the MM, the (unsigned) OSF falls to about 10^{14} Wb, which should be compared to values around 10^{15} Wb at the peaks of recent solar cycles. Thus the Earth's residence times in fast or intermediate flows would be an order of magnitude shorter in the MM than during recent solar cycles and enhancements in mean solar wind speeds would therefore be of order a tenth that in recent cycles, i.e. of order 25 km s^{-1}, if fast and slow solar wind speeds remained the same and changes are all caused by variations in Earth's residence times in such flow regimes. Therefore we conclude that solar wind speeds would be relatively uniform in the MM (between about 250 and 275 km s^{-1}, i.e. roughly half the average seen in modern times).

The authors are grateful to many scientists for the provision of the many types of data used in this Letter.

REFERENCES

Barnard, L., Lockwood, M., Hapgood, M. A., et al. 2011, GeoRL, 38, L16103
Cliver, E.W., & Ling, A. G. 2011, SoPh, 274, 285
de Toma, G. 2011, SoPh, 274, 195
Finch, I., Lockwood, M. L., & Rouillard, A. P. 2008, GeoRL, 35, L21105
Judge, P. G., & Saar, S. H. 2007, ApJ, 663, 643
Lockwood, M. 2013, LRSP, 10, 4
Lockwood, M., Barnard, L., Nevanlinna, H., et al. 2013a, AnGeo, 31, 1957
Lockwood, M., Barnard, L., Nevanlinna, H., et al. 2013b, AnGeo, 31, 1979
Lockwood, M., Owens, M., Barnard, L., Davis, C., & Thomas, S. 2012, A&G, 53, 3.09
Lockwood, M., Rouillard, A. P., & Finch, I. D. 2009, ApJ, 700, 937
Lockwood, M., Stamper, R., & Wild, M. N. 1999, Natur, 399, 437
Lockwood, M., Nevanlinna, H., Vokhmyanin, M., et al. 2014, Reconstruction of Geomagnetic Activity and Near-earth Interplanetary Conditions over the Past 167 Years: Improved Representation of Solar Cycle 11, AnGeo, submitted
Manoharan, P. K. 2012, ApJ, 751, 128
Owens, M. J., Crooker, N. U., & Lockwood, M. 2011, JGRA, 116, A04111
Owens, M. J., Crooker, N. U., & Lockwood, M. 2013, JGRA, 118, 1868
Owens, M. J., & Lockwood, M. 2012, JGRA, 117, A04102
Owens, M. J., Usoskin, I., & Lockwood, M. 2012, GeoRL, 39, L19102
Owens, M. J., Crooker, N. U., & Lockwood, M. 2014, Solar Cycle Evolution of the Dipolar and Pseudostreamer Belts and their Relation to the Slow Solar Wind, JGRA, in press
Pevtsov, A. A., Fisher, G. H., Acton, L. W., et al. 2003, ApJ, 598, 1387
Riley, P., & Luhmann, J. G. 2012, SoPh, 277, 355
Riley, P., Mikic, Z., Lionello, R., et al. 2010, JGRA, 115, A06104
Rouillard, A., Lockwood, M., & Finch, I. 2007, JGRA, 112, A05103
Schwadron, N. A., & McComas, D. J. 2003, ApJ, 599, 1395
Schwadron, N. A., McComas, D. J., & DeForest, C. 2006, ApJ, 642, 1173
Solanki, S., Schüssler, M., & Fligge, M. 2000, Natur, 408, 445
Steinhilber, F., Abreu, J. A., Beer, J., & McCracken, K. G. 2010, JGRA, 115, A01104
Svalgaard, L. 2013, Errors in Scale Values for Magnetic Elements for Helsinki, AnGeo, submitted
Svalgaard, L., Cliver, E. W., & Kamide, Y. 2005, GeoRL, 32, L01104
Svalgaard, L., Cliver, E. W., & Lesager, P. 2003, in Solar Variability as an Input to the Earth's Environment, Determination of Interplanetary Magnetic Field Strength, Solar Wind Speed and Euv Irradiance, 1890–2003, ed. A. Wilson (ESA SP-535; Noordwijk: ESA), 15
Usoskin, I. 2013, LRSP, 10, 1